A&A 476, 291–300 (2007)
DOI: 10.1051/0004-6361:20078502

Astronomy & Astrophysics

Formation, fractionation, and excitation of carbon monoxide in diffuse clouds

H. S. Liszt

National Radio Astronomy Observatory, 520 Edgemont Road, Charlottesville, VA, 22903-2475, USA
e-mail: hliszt@nrao.edu

Received 18 August 2007 / Accepted 3 October 2007

ABSTRACT

Context. A wealth of observations of CO in absorption in diffuse clouds has accumulated in the past decade at *uv* and mm-wavelengths
Aims. Our aims are threefold: a) To compare the *uv* and mm-wave results; b) to interpret ^{13}CO and ^{12}CO abundances in terms of the physical processes which separately and jointly determine them; c) to interpret observed $J = 1-0$ rotational excitation and line brightness in terms of ambient gas properties.
Methods. A simple phenomenological model of CO formation as the immediate descendant of quiescently-recombining HCO^+ is used to study the accumulation, fractionation and rotational excitation of CO in more explicit and detailed models of H_2-bearing diffuse/H I clouds
Results. The variation of N(CO) with $N(H_2)$ is explained by quiescent recombination of a steady fraction $n(HCO^+)/n(H_2) = 2 \times 10^{-9}$. Observed $N(^{12}CO))/N(^{13}CO)$ ratios generally do not require a special chemistry but result from competing processes and do not provide much insight into the local gas properties, especially the temperature. $J = 1-0$ CO line brightnesses directly represent N(CO), not $N(H_2)$, so the CO-H_2 conversion factor varies widely; it attains typical values at $N(^{12}CO) \lesssim 10^{16}$ cm^{-2}. Models of CO rotational excitation account for the line brightnesses and CO-H_2conversion factors but readily reproduce the observed excitation temperatures and optical depths of the rotational transitions only if excitation by H-atoms is weak – as seems to be the case for the very most recent calculations of these excitation rates.
Conclusions. Mm-wave and *uv* results generally agree well but the former show somewhat more enhancement of ^{13}C in ^{13}CO. In any case, fractionation may seriously bias $^{12}C/^{13}C$ ratios measured in CO and other co-spatial molecules. Complete C→CO conversion must occur over a very narrow range of A_V and $N(H_2)$ just beyond the diffuse regime. For $N(H_2) < 7 \times 10^{19}$ cm^{-2} the character of the chemistry changes inasmuch as CH is generally undetected while CO suffers no such break.

Key words. astrochemistry – molecular processes – ISM: clouds – ISM: molecules

1. Introduction

Except for hydrogen, carbon monoxide is the most important and widely observed molecule in the interstellar medium (ISM). The 7−8 decade span in column density over which CO is directly observed, from N(CO) = 10^{12} cm^{-2} in *uv* absorption in the diffuse interstellar medium to N(CO) > 10^{19} cm^{-2} in mm and sub-mm emission from dense and giant molecular clouds, is exceeded only by that of H_2 itself. The ubiquity of CO has encouraged the use of mm-wave CO emission as a possible tracer of molecular hydrogen even into such extreme environments as high velocity clouds (Dessauges-Zavadsky et al. 2007).

Interpreting observations of CO in diffuse gas (Snow & McCall 2006) over the lower half of its range, at N(CO) $\lesssim 10^{16}$ cm^{-2}, has been particularly challenging. The fraction of free gas-phase carbon in CO is small, a few percent or less when, locally, $A_V < 1$ mag, but it is still 30−50 times larger than can be explained by the quiescent gas-phase ion-molecule chemistry of low-density media like diffuse clouds (Van Dishoeck & Black 1988; Warin et al. 1996). The relative abundance of CO with respect to H_2 varies widely in this regime (see Fig. 1; with much scatter, approximately as $N(CO) \propto N(H_2)^2$ over the range $X(CO) = N(CO)/N(H_2) \approx 3 \times 10^{-8}-3 \times 10^{-5}$) and the relative abundances of ^{12}CO and ^{13}CO are strongly affected by fractionation (Watson et al. 1976; Smith & Adams 1980) such that $20 \lesssim N(^{12}CO)/N(^{13}CO) \lesssim 170$ (see the references cited in Sect. 2).

Despite the comparatively small CO abundances in diffuse clouds, λ 2.6 mm $J = 1-0$ rotational emission is often appreciable. Typically it is seen that $T_B \approx 1-5$ K, $W_{CO} \approx 1-5$ K km s^{-1} peak or integrated brightness for N(CO) = $10^{15}-10^{16}$ cm^{-2} (Liszt & Lucas 1998) but peak brightnesses as high as 10−13 K have been observed (Liszt & Lucas 1994). Moreover, the $J = 1-0$ rotational transition may have appreciable optical depth in diffuse gas because its excitation is quite weak. Surveys of ^{12}CO alone may be hard-pressed to distinguish between dark and diffuse gas, especially at higher galactic latititude or larger galactocentric radii owing to the broader distribution of diffuse gas.

To elucidate the properties of CO in the diffuse regime, we discuss here a wealth of observational material at *uv* and mm-wavelengths which has accumulated (much of it very recently) over the past decade. The plan of this work is as follows. Section 2 gathers the previously-published observational results (Liszt & Lucas 1998; Sonnentrucker et al. 2007; Burgh et al. 2007; Sheffer et al. 2007) which form the basis of the present discussion. Section 3 displays and discusses the run of observed values of the CO and H_2 column densities to demonstrate that there is at least a phenomenological basis for understanding the abundance of CO in diffuse gas, in order to show that there is some knowledge of the microscopic CO formation rate. This rate and those of the various other physical processes which account for the abundances of ^{12}CO and ^{13}CO are set out in detail in Sect. 4. Section 5 discusses the observed abundances of ^{12}CO

and ^{13}CO and their fractionation, and Sect. 6 discusses the rotational excitation and brightness of the $J = 1-0$ rotational transition. Section 7 is a brief discussion and summary of outstanding concerns.

2. Observational material

With one minor exception (see Sect. 6), the discussion here relies on previously-published results in the *uv* and mm-wavelength regimes, as we now discuss.

2.1. uv and optical absorption

Many determinations of N(CO) and $N(H_2)$ have recently been published by Sonnentrucker et al. (2007), Burgh et al. (2007) and Sheffer et al. (2007), who provide measurements of $N(H_2)$, $N(^{12}CO)$ and $N(^{13}CO)$, along with such additional physically interesting quantities as the $J = 1-0$ rotational temperatures of H_2 and/or carbon monoxide and, from Sonnentrucker et al. (2007), column densities and related quantities for such species as CH and C_2. For the lines of sight where there is overlap, agreement is generally excellent for the column densities of CO and H_2 and only slightly worse for the CO excitation temperature, as shown below in Figs. 5 and 6. In cases of overlap, we chose values from the reference with the smaller quoted errors if the datasets were equally comprehensive in that direction. However, we also chose not to mix values for $N(^{12}CO)$ and $N(^{13}CO)$ from different references along any given line of sight, because the systematic errors could be different.

2.2. MM-wave absorption

Observations of carbon monoxide in absorption toward mm-wave continuum sources were given by Liszt & Lucas (1998), along with rotational excitation temperatures and isotope ratios, etc.). $N(H_2)$ is not known directly in these measurements, which assume instead that $N(H_2) = N(HCO^+)/2 \times 10^{-9}$ (Liszt & Lucas 1996; Lucas & Liszt 1996, 2000). The current discussion may be regarded as a consistency check on this assumption.

In comparing the radio and optical lines of sight, it should be remembered that the former use extragalactic background sources, penetrate the entire galactic layer, and refer to individual, well-resolved kinematic components. The optical/*uv* lines of sight stop within the Galaxy and are sums over undifferentiated – though not necessarily blended – features for species studied in the *uv*, that is for CO and H_2.

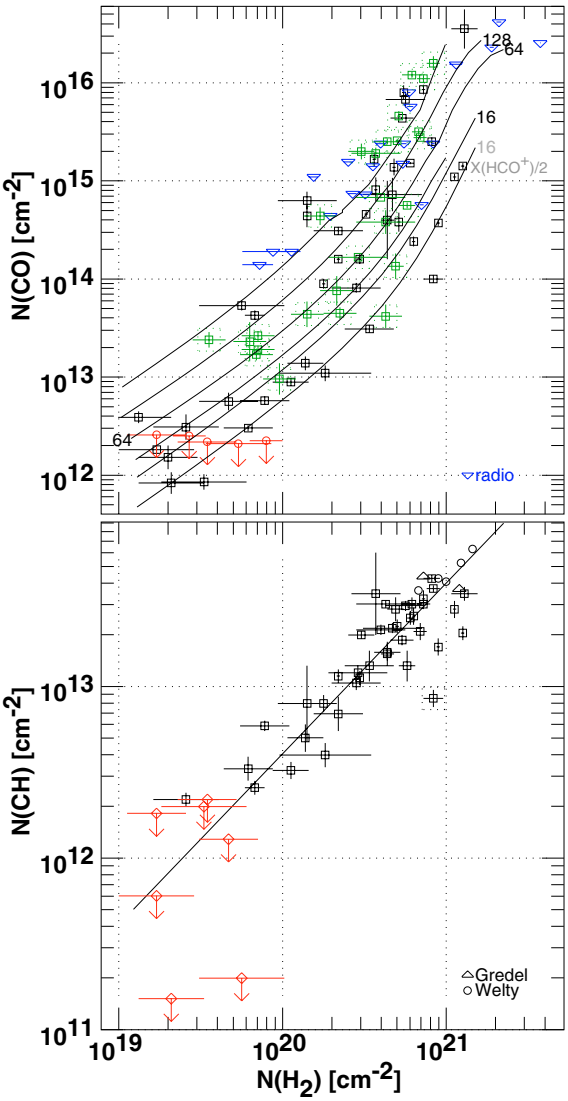

Fig. 1. *Top*: variation of CO and H_2 column densities observed in *uv* (rectangles; Sonnentrucker et al. 2007; and Burgh et al. 2007) and mm-wave (triangles; Liszt & Lucas 1998) CO absorption. Lines of sight represented in Fig. 5 are outlined and shown in green. For the mm-wave data $N(H_2) = N(HCO^+)/2 \times 10^{-9}$. The curves represent models of CO formation *via* recombination of HCO^+ and are labelled by their density $n(H) \approx n(H\ I) + 2n(H_2)$ (see Sect. 4). The lowest curve shows the result of halving the HCO^+ abundance at $n(H) = 16$ cm^{-3}. *Bottom*: variation of CH and H_2 column densities from the summary tables of Sonnentrucker et al. (2007) and a few high-N(CH) datapoints from Gredel et al. (1993) and Welty et al. (2003).

3. Variation of molecular abundance with H_2 and the source function for carbon monoxide

The abundances of ^{12}CO and ^{13}CO are the result of several processes; chemical formation and destruction, carbon isotope exchange and (selective) photodissociation. Interpreting the observations requires an understanding of the competing influences of all such processes, but the overall guage is really set by a comparison of the photodissociation rate (which is known in free space and calculable within a model) and the direct chemical formation rate. Once the latter is specified, other physical properties follow directly and it is even possible to model the internal rotational excitation and predicted mm-wave brightness. Here we outline an empirical approach to estimating the rate of CO formation.

3.1. CO and H_2

In Fig. 1 at top we show the observed run of $N(^{12}CO)$ with $N(H_2)$. The rise of N(CO) with increasing $N(H_2)$ is very steep, approximately $N(CO) \propto N(H_2)^2$, with scatter amounting to two orders of magnitude at fixed $N(H_2)$. At each $N(H_2)$ the radio-derived N(CO) is comparatively but not inordinately large; this could be an indication that $X(HCO^+)$, taken as 2×10^{-9}, has been slightly overestimated. The large subset of *uv*-absorption datapoints which have CO excitation temperature measurements and which therefore appear also in Fig. 5 have been flagged and colored green in Fig. 1, in order to highlight the fact that most

of them require model densities of at least $n(\mathrm{H}) = 64$ cm^{-3} (see Sect. 6).

What to make of the variation of $N(\mathrm{CO})$ with $N(\mathrm{H_2})$? Models of CO formation employing thermal processes in quiescent diffuse gas have largely been unable to reproduce observed values of $X(\mathrm{CO})$ except perhaps at rather higher densities than are otherwise inferred for diffuse gas; see Fig. 16 of Sonnentrucker et al. (2007). However, purely phenomenologically, it is known that thermal gas-phase electron recombination of the observed amount of $\mathrm{HCO^+}$, $X(\mathrm{HCO^+}) \approx 2 \times 10^{-9}$, does suffice to reproduce the observed $X(\mathrm{CO})$ at modest densities. This is shown by the curves at the top in Fig. 1, where, updating the calculations of Liszt & Lucas (2000), we plot the predicted $N(\mathrm{CO})$ for diffuse cloud models in which an artificially steady relative abundance $X(\mathrm{HCO^+}) = 2 \times 10^{-9}$ is allowed to recombine with free electrons at the thermal rate; note that the mm-wave observations of $N(\mathrm{CO})$ and $N(\mathrm{HCO^+})$ have been placed in the plane of the figure by relying on the same $X(\mathrm{HCO^+})$ which in the models explains the CO abundance.

The models are for small uniform density spheres immersed in the mean galactic radiation fields, within which the thermal balance, ionization equilibrium and $\mathrm{H_2}$ and CO accumulation problems are solved self-consistently (Liszt 2007) using the self-shielding factors of Lee et al. (1996). For each total density $n(\mathrm{H}) = 16$, 32, 64 ... 256 cm^{-3}, a series of models of increasing $N(\mathrm{H})$ was calculated, and the CO and $\mathrm{H_2}$ column densities across the central line of sight were calculated to form the curves for each $n(\mathrm{H})$.

The newer calculations differ from the older ones in a variety of small ways, for instance the rates for O I and C I excitation by hydrogen atoms were very recently recalculated by Abrahamsson et al. (2007). Most important is the recognition, following observation of $\mathrm{H_3^+}$, and accounting for the neutralization rate on small grains/PAH, that the low-level hard ionization rate of hydrogen, presumably due to cosmic rays, is apparently larger in diffuse gas (McCall et al. 2002; Liszt 2003). This has the effect of increasing the densities of $\mathrm{H^+}$ and $\mathrm{He^+}$ and the overall electron fraction (which, however, is never more than about twice the free carbon abundance). Higher electron fractions lead to more rapid formation of CO (if CO forms by $\mathrm{HCO^+}$ recombination) while the increased density of $\mathrm{He^+}$ plays an elevated role in the destruction of carbon monoxide. Indeed, destruction by $\mathrm{He^+}$ is the dominant *chemical* mechanism for ^{12}CO destruction. The various processes responsible for destroying CO are discussed in Sect. 4.

In the figure, scatter in $N(\mathrm{CO})$ at fixed $N(\mathrm{H_2})$ is implicitly attributed to variations in density, which in the models ranges between $n(\mathrm{H}) = 16$ cm^{-3} and 256 cm^{-3}. However, the very lowest curve shows the result of halving $X(\mathrm{HCO^+})$ in the model and additional observational scatter, perhaps substantial, could also result from variations in geometry and ambient illumination. Consideration of fractionation strongly suggests variations of a factor two or more in the photodissociation rate (see Sect. 5 and Fig. 4).

In the remainder of this work we will assume that the direct CO formation rate is adequately specified by the dissociative recombination of $\mathrm{HCO^+}$ at $X(\mathrm{HCO^+}) = 2 \times 10^{-9}$ and we will employ this as a basis to interpret the observed fractionation and rotational excitation in a self-consistent fashion (interpreting brightness, etc. within the context of a model which also accounts for the abundance). The following section sets out in detail the physical processes which determine the abundances of ^{12}CO and ^{13}CO.

3.2. CO, CH and H_2

By contrast with CO, the variation of $N(\mathrm{CH})$ with $N(\mathrm{H_2})$ is very nearly linear and with considerably smaller scatter and overall range for the actually-measured $N(\mathrm{CH})$. Figure 1 at bottom is an updated version of Fig. 1 of Liszt & Lucas (2002) and although it shows a somewhat less-perfect correlation in a larger dataset (46 vs. 32 sightlines), the derived means $\langle N(\mathrm{CH})\rangle/\langle N(\mathrm{H_2})\rangle = 4.1 \times 10^{-8}$ and $\langle N(\mathrm{CH})/N(\mathrm{H_2})\rangle = 4.5 \pm 1.6 \times 10^{-8}$ (for lines of sight with CH detections at $N(\mathrm{H_2}) \geq 7 \times 10^{19}$ cm^{-2}) are nearly unchanged, $N(\mathrm{CH})$ and $N(\mathrm{CO})$ are well-correlated (coefficient 0.86; this is somewhat contrary to a remark by Crenny & Federman 2004) though the functional relationship is quite steep, $N(\mathrm{CO}) \propto N(\mathrm{CH})^{2.6}$.

In general, for $N(\mathrm{CH}) > 2 \times 10^{12}$ cm^{-2}, CH is a quite reliable indicator of the $\mathrm{H_2}$ column density, with $N(\mathrm{H_2}) \approx N(\mathrm{CH})/4 \times 10^{-8}$. However, and somewhat remarkably, for $N(\mathrm{H_2}) < 7 \times 10^{19}$ cm^{-2} it is somewhat more likely to find CO than CH, and several lines of sight at lower $N(\mathrm{H_2})$ have very high values of $N(\mathrm{CO})/N(\mathrm{CH})$ (see Fig. 18 in Sonnentrucker et al. 2007). Lines of sight with low molecular abundances, including a few of those with smaller or undetected $N(\mathrm{CH})$ in Fig. 1, were discussed by Zsargó & Federman (2003), who argued that non-thermal processes must preferentially dominate the chemistry along some very transparent lines of sight. Alternatively we noted that very high values for $X(\mathrm{OH}) = N(\mathrm{OH})/N(\mathrm{H_2})$ might be expected in more diffuse $\mathrm{H_2}$-bearing gas just from quiescent thermal processes (Liszt 2007); if CO is formed from OH, high $N(\mathrm{CO})/N(\mathrm{CH})$ ratios might also be explained in this way.

4. Mechanisms of CO formation and fractionation

In this section we set out the various physical processes contributing to the formation, destruction and fractionation of carbon monoxide, albeit in a very reductive fashion. The ambient gas is taken to be diffuse but purely molecular and the molecular abundances are taken to be small enough that conservation of nuclei need not be explictly observed; that is, the fraction of C in CO is not large enough to affect the relative abundance of $\mathrm{HCO^+}$ and the fraction of ^{13}C in ^{13}CO is not large enough to alter the relative rates at which ^{12}CO and ^{13}CO form from the isotopic variants of $\mathrm{HCO^+}$.

4.1. Source function for carbon monoxide formation

As noted above, a source function for carbon monoxide may be approximated as the quiescent thermal recombination rate of a fixed relative abundance $X(\mathrm{HCO^+}) = 2 \times 10^{-9}$ such that the observations are explained at densities typical of diffuse clouds, even if the exact formation route for $\mathrm{HCO^+}$ in diffuse gas is problematical. Ion-molecule reactions in such a quiescent gas form too little $\mathrm{HCO^+}$ and/or CO by a factor of about 30 and to account for the discrepancy it has been suggested that chemical reactions with $\mathrm{C^+}$ are driven at higher rates for various reasons. The carbon isotope exchange reactions also involve $\mathrm{C^+}$ and it is of interest to ask whether they also must be driven at non-thermal rates in order to account for the observed $N(^{12}\mathrm{CO})/N(^{13}\mathrm{CO})$ ratios.

The rate constant for thermal recombination of $\mathrm{HCO^+}$ with electrons is 3.3×10^{-5} cm^3 s$^{-1}/T_\mathrm{K}$ according to the UMIST reaction rate database (Woodall et al. 2007); therefore the volume formation rate of ^{12}CO due to recombination of $\mathrm{H}^{12}\mathrm{CO^+}$ in a gas having an electron fraction $X(\mathrm{e}) = n(\mathrm{e})/n(\mathrm{H_2})$ is

$$\mathrm{d}n(^{12}\mathrm{CO})/\mathrm{d}t = 6.6 \times 10^{-14}\, X(\mathrm{e}) n(\mathrm{H_2})^2 \ \mathrm{cm^{-3}\ s^{-1}}/T_\mathrm{K}$$

and the formation rate of ^{13}CO due to recombination of $H^{13}CO^+$ is here taken to be 60 times smaller following our isotope measurements in mm-wave absorption (Lucas & Liszt 1998).

4.2. Carbon isotope exchange

^{12}CO molecules are interconverted to ^{13}CO with a rate constant k_f by the reaction $^{13}C^+ + {}^{12}CO \rightarrow {}^{12}C^+ + {}^{13}CO + 34.8$ K, and in the other direction at rate $k_r = k_f \exp(-34.8/T_K)$ (Watson et al. 1976). The rate constants were measured by Smith & Adams (1980) and shown to be strongly temperature-dependent below 500 K with a measured value $k_f = 7 \times 10^{-10}$ cm^3 s^{-1} at $T_K = 80$ K, (and an implied value 70% larger at 10 K), as compared with $k_f = 2 \times 10^{-10}$ cm^3 s^{-1} measured at $T_K = 300$ K by Watson et al. (1976). Smith & Adams (1980) discuss the means by which to convert their measurements to values of k_f below 80 K and their results have been employed by most subsequent authors, for instance Chu & Watson (1983) or Langer et al. (1984) (although not by Sheffer et al. (2007) who used the much smaller value of Watson et al. (1976), claiming that it agreed better with observation).

A suitable expression for $k_f(T_K)$ based on the results of Smith & Adams (1980) does not exist in the literature. For future reference, we provide the following:

$$k_f = 7.64 \times 10^{-9}\ T_K{}^{-0.55}\ \mathrm{cm^3\ s^{-1}}\ \ (T_K = 80\text{–}500\ \mathrm{K}) \tag{4a}$$

$$k_f = \frac{1.39 \times 10^{-9}\ T_K{}^{-0.05}\ \mathrm{cm^3\ s^{-1}}}{1 + \exp(-34.8/T_K)}\ \ (T_K = 10\text{–}80\ \mathrm{K}). \tag{4b}$$

In terms of volume formation rates, the forward reaction forming ^{13}CO proceeds at a volume rate

$$dn(^{13}CO)/dt = k_f\ X(^{12}CO)\ X(^{13}C^+)\ n(H_2)^2\ \mathrm{cm^{-3}\ s^{-1}}.$$

It is straightforward to show that the backward reaction between $^{12}C^+$ and ^{13}CO is never an important "source" of ^{12}CO (given the rate at which ^{12}CO putatively forms from $H^{12}CO^+$) but conversion of ^{12}CO to ^{13}CO is the dominant route to ^{13}CO formation when the relative abundance $X(^{12}CO)$ substantially exceeds 10^{-6}. The ^{13}C-insertion reaction would dominate at much smaller $X(^{12}CO)$ if the direct formation rates were slower, leading to problems making models with $X(^{12}CO)/X(^{13}CO) \gg 60$, as in Fig. 16 of Warin et al. (1996) (at far left).

4.3. Destruction of carbon monoxide by He^+

The reaction $He^+ + CO \rightarrow C^+ + O + He$ proceeds with a rate constant $k_{He} = 1.6 \times 10^{-9}$ cm^3 s^{-1} and is the dominant *chemical* destruction mechanism for ^{12}CO whenever $n(H_2) < 100$ cm^{-3}. [1] Calculation of the ionization equilibrium is complicated, but diffuse cloud models tend to produce a nearly constant *number density* of He^+ because such a large fraction of the free electrons arises from the near-complete photoionization of carbon. From our models we take $n(He^+) = 3.4 \times 10^{-4}$ cm^{-3} which is appropriate either when neutralization by small grains is considered and $\zeta_H = 2 \times 10^{-16}$ s^{-1} per H-nucleon or when neutralization by small grains is ignored and $\zeta_H = 10^{-17}$ s^{-1} (Liszt 2003).

The volume destruction rate of ^{12}CO by He^+ is $dn(^{12}CO)/dt = -k_{He}\ n(He)^+ n(^{12}CO)\ \mathrm{cm^{-3}\ s^{-1}}$ or, numerically

$$dn(^{12}CO)/dt = -5.4 \times 10^{-13}\ X(^{12}CO)\ n(H_2)\ \mathrm{cm^{-3}\ s^{-1}}.$$

[1] The same is not true for ^{13}CO, whose chemical destruction is generally dominated by ^{12}C-insertion whenever $n(H_2) > 2$ cm^{-3}, see Eqs. (4c) and (4d).

4.4. Photodestruction and selective photodissociation

The nominal free-space photodissociation rate in the mean interstellar radiation field is usually taken to be the same for either version of CO and we parameterize the photodestruction rate internal to a cloud as 2.1×10^{-10} s^{-1} $g_Y\ I$ where $I \langle\rangle 1$ represents the possibility of a variable external radiation field, 2.1×10^{-10} s^{-1} is the photodissociation rate in free space (Le Teuff et al. 2000), and g_{12} or g_{13} represent the diminution of the photodestruction rate due to shielding by dust, H_2 and other carbon monoxide molecules for either isotope. The free-space rates for ^{12}CO and ^{13}CO are taken equal but g_{12} declines more rapidly into a cloud than does g_{13} (Van Dishoeck & Black 1988; Warin et al. 1996). In Sect. 5 we show an example where this behaviour is parametrized as $g_{13} = g_{12}^{0.6}$.

4.5. Relative abundances of ^{12}CO and ^{13}CO

Given the preceding considerations in this Section we may write the following approximate, implicit and local expressions for the relative abundances

$$X(^{12}CO) = \frac{1.2 \times 10^{-7} X(e)' n(H_2)/T_K}{g_{12} I + 0.0026 + 2.3 \times 10^{-5} k_f' n(H_2)} \tag{4c}$$

$$X(^{13}CO) = \frac{(2.0 \times 10^{-9} X(e)'/T_K + 2.3 \times 10^{-5} X(^{12}CO)) n(H_2)}{g_{13} I + 0.0026 + 0.0014 k_f' n(H_2) \exp(-34.8/T_K)} \tag{4d}$$

where $k_f' = k_f/10^{-9}$ cm^3 s^{-1}, I measures the strength of the incident interstellar radiation field normalized to its mean strength ($I = 1$) and $X(e)' = X(e)/4 \times 10^{-4}$; the electron fraction is comprised of a contribution from fully once-ionized atomic carbon at the level of 3.2×10^{-4} for an H_2 gas (Sofia et al. 2004), and the remainder from H^+ due to cosmic-ray ionization (Liszt 2003). The first term in the numerator of Eq. (4d) corresponds to recombination of $H^{13}CO^+$ with $X(H^{12}CO^+)/X(H^{13}CO^+) = 60$ and the numerical constant in both denominators represents destruction by interaction with He^+. In considering these expressions note that the hydrogen in diffuse gas is not wholly molecular, probably even when CO is detected, and the total density $n(H) = n(H\ I) + 2\ n(H_2) = 2\ n(H_2)/f_{H_2}$ where f_{H_2} is the fraction of H-nuclei in H_2.

Note the following with regard to these expressions. For ^{12}CO, photodestruction is dominant until $g_{12}\ I \approx 0.003$, at which point the shielding would be strong enough to permit near-complete conversion of carbon to CO. Thus this simple chemical scheme can carry the gas from the diffuse to the dark regime (where the free carbon abundance is somewhat lower and $X(^{12}CO) \approx 10^{-4}$). Also for ^{12}CO, destruction by conversion to ^{13}CO dominates over destruction by He^+ only for $n(H_2) > 100$ cm^{-2}; this stands in opposition to the situation for ^{13}CO, where the interaction with He^+ is negligible at almost all densities. This imbalance contributes to the lack of equilibration of the carbon isotope exchange, complicating the interpretation of the observed $^{12}CO/^{13}CO$ ratios,

Finally, note that conversion from ^{12}CO becomes the dominant source of ^{13}CO only when $X(^{12}CO) > 10^{-4}/T_K$ or $X(^{12}CO) > 2 \times 10^{-6}$. If the direct formation rate of carbon monoxide were taken to be much smaller than that given here, as is the case in models which substantially fail to reproduce the overall carbon monoxide abundance, conversion from ^{12}CO would dominate the formation of ^{13}CO at far smaller $X(^{12}CO)$. This would make it very make it very difficult to reproduce ratios $N(^{12}CO)/N(^{12}CO) \gg 60$, which require strong self-shielding of the ^{12}CO and therefore, high $X(^{12}CO)$ (see Sect. 5.2).

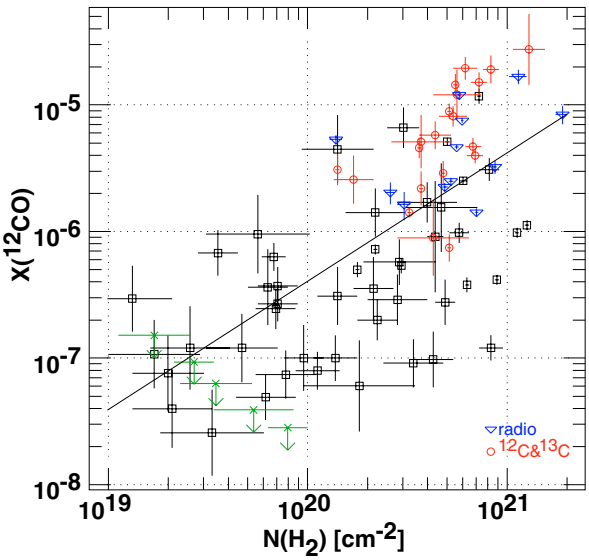

Fig. 2. Variation of $X(^{12}CO) = N(^{12}CO)/N(H_2)$ with $N(H_2)$. The regression line shown has slope 1.014 ± 0.13 and passes through $X(^{12}CO) = 4.05 \times 10^{-7}$ for $N(H_2) = 10^{20}$ cm^{-2}. Lines of sight having *uv* absorption measurements of both ^{12}CO and ^{13}CO are noted (red in appropriate media); they have relatively high $X(^{12}CO)$ at a given $N(H_2)$.

5. Observed $N(^{12}CO)$ and $N(^{13}CO)$

5.1. X(CO) at the extremes of abundance

Figure 2 shows the observed variation of $X(^{12}CO)$ with $N(H_2)$; with much scatter, the regression line has unit slope (see the caption); Fig. 20 of Sonnentrucker et al. (2007) appeared to show that $X(^{12}CO) \approx 5 \times 10^{-8}$, independent of $N(H_2)$, for most lines of sight at $N(H_2) < 3 \times 10^{20}$ cm^{-2}.

5.1.1. The low-abundance limit

Considering the smallest observed CO column densities and abundances, at $N(H_2) \leq 3 \times 10^{19}$ cm^{-2}, $\langle X(^{12}CO)\rangle \approx 8 \times 10^{-8}$ (Fig. 2). In light of Eq. (4c), we note that $n(H)/T_K \approx 1$ in diffuse gas, for instance, $n(H) = 50$ cm^{-3}, $T_K = 50$ K yields a typical thermal pressure in the ISM, but $n(H_2)/n(H) < 1$ in such a gas. Thus even our high ad hoc formation rate for CO predicts $X(^{12}CO)$ somewhat below 10^{-7} in unshielded regions $g_{12} = 1$ and the observed CO is likely to be largely unshielded at the lowest observed $N(H_2)$. Gas observed at $N(H_2) > 10^{20}$ cm^{-2}, $X(^{12}CO) > 10^{-7}$ must generally be substantially self-shielded in ^{12}CO, implying that the observed $N(^{12}CO)/N(^{13}CO)$ do not directly reflect the interstellar isotope ratio.

5.1.2. High X(CO)

Complete conversion of carbon to CO in a fully molecular diffuse gas would yield $X(^{12}CO) = 3.2 \times 10^{-4}$ given the free gas phase abundance of carbon determined by Sofia et al. (2004), implying that the highest observed fractions of carbon in carbon monoxide in the molecular portion of the gas are $[^{12}CO]/[^{12}C] \approx 0.08$. These fractions are small enough to ensure that the observed gas may truly be considered diffuse, with nearly all carbon in the form of C^+, but they are not necessarily small enough that their effects on other species are completely ignorable.

For ^{13}C, the fraction in ^{13}CO may be substantially higher owing to fractionation, reaching 0.20–0.25 (see just below). In this case, the ambient molecular gas is appreciably deprived of free ^{13}C-nuclei, and account should be taken of such effects on the isotope ratios derived from other species like CH which are expected to share the same volume as CO. Such sharing is somewhat less obvious for CH^+ but in general, it seems clear that carbon isotope measurements in the diffuse ISM should avoid sightlines having substantial CO, unless the bias caused by carbon monoxide fractionation can be corrected somehow. It seems generally to be the case that the more pronounced effect of CO fractionation is to deprive the ambient gas of ^{13}C but, if it were observed that $N(^{12}CO)/N(^{13}CO) \gg 60$ at sufficiently high $X(^{12}CO)$, the opposite would be the case.

Again considering Eq. (4c), but in the limit of large $X(CO)$, $X(CO) \rightarrow 4.7 \times 10^{-3}/T_K$ in the limit of high $n(H_2)$ and strong shielding ($I\, g_{12} \rightarrow 0$) or $X(^{12}CO) \approx 10^{-4}$ at $T_K = 40$ K. Noting the behaviour in Figs. 1 and 2 we infer that this high-abundance limit would occur only for $N(H_2) \gg 3 \times 10^{21}$ cm^{-2}, $N(^{12}CO) \approx 3 \times 10^{17}$ cm^{-2}, well above the observed range. $X(^{12}CO) = 10^{-4}$ is still a factor of three below the free-carbon fraction relative to H_2 in diffuse molecular gas. In the observed diffuse sightlines, the destruction of ^{12}CO is dominated by photodissociation so that $Ig_{12} \gtrsim 0.01$ even at the largest $N(H_2)$ and $N(^{12}CO)$.

5.2. Fractionation

Figure 3 shows a summary of available measurements of the two most abundant forms of carbon monoxide observed in absorption in diffuse clouds. Sheffer et al. (2007) noted that lines of sight studied in ^{13}CO have about 20 K lower H_2 $J = 1–0$ rotational temperatures than the mean for all H_2 surveyed. As indicated in Fig. 2, the sightlines examined in ^{13}CO in *uv* absorption are nearly always those with the very highest $X(^{12}CO)$ at a given $N(H_2)$, and to that extent are not entirely representative even though they vary widely in column density.

The data show $N(^{12}CO)/N(^{13}CO)$ ratios in the range $15 < N(^{12}CO)/N(^{13}CO) < 170$ and a tendency for the ratio to decline with increasing column density and/or relative abundance $X(CO)$, but with much scatter. There is no tendency for the ratio to decline with the rotational temperature of H_2 as noted in the figure but the two lines of sight with the smallest ratios studied optically are those with very much the lowest temperature indicated by C_2. The radio data consistently find smaller ratios at a given column density but the effect is more pronounced in the panel at right. There has been something of a recent convergence between the radio and *uv* absorption studies in that the latter have only now found lines of sight where $N(^{12}CO)/N(^{13}CO) \ll 60$, as was often found to the case in mm-wavelength absorption (Liszt & Lucas 1998). Previously, optical absorption studies occured only along lines of sight having much larger ratios (Lambert et al. 1994; Federman et al. 2003) and this disparity was the source of some concern.

The expected functional behaviour of the column density ratio is as follows; at very low $N(H_2)$ and/or $N(CO)$ the gas is unshielded, the photodissociation rates are assumed equal and the observed $N(^{12}CO)/N(^{13}CO)$ ratios should be very near the ratio of formation rates, presumably $[^{12}C]/[^{13}C] = 60$ (Lucas & Liszt 1998). However, as indicated in Fig. 2, the lines of sight chosen for study of the isotope ratio have such high CO abundances that they do not sample the unshielded regime. At intermediate $X(CO)$ and $N(CO)$, self- shielding increases the contribution of isotope exchange to ^{13}CO formation at $X(^{12}CO) > 2 \times 10^{-6}$, but also increases the disparity between g_{12} and g_{13}. Therefore, at intermediate $X(CO)$ the column density ratio $N(^{12}CO)/N(^{13}CO)$ can be expected to be both above and below the intrinsic isotope

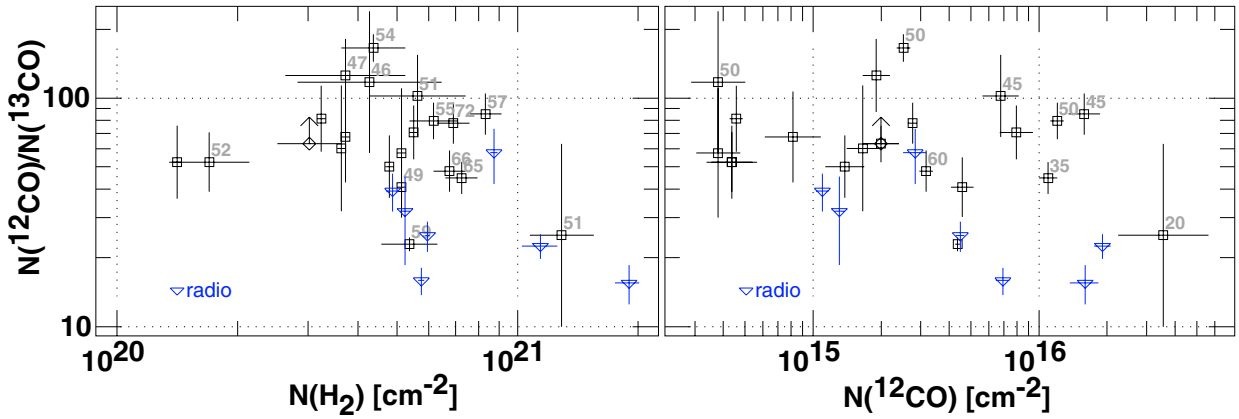

Fig. 3. *Left*: variation of $N(^{12}CO)/N(^{13}CO)$ with $N(H_2)$ (*left*) and $N(^{12}CO)$. Where possible points are labeled with estimates of T_K from H_2 (*at left*) and C_2 (*right*) as tabulated by Burgh et al. (2007) and Sheffer et al. (2007) for H_2 and Sonnentrucker et al. (2007) for H_2 and C_2. Radiofrequency data are those of Liszt & Lucas (1998). There is no tendency for the column density ratio to vary monotonically with the H_2 temperature and only a very loose trend with that of C_2.

ratio in the gas, with the very lowest values at larger N(CO). Finally, at very high N(CO), the column density ratio must tend toward the intrinsic isotope ratio when all ^{12}C resides in ^{12}CO but this regime again is well beyond the scope of the present dataset.

In order that the forward and backward isotope insertion reactions equilibrate, the rightmost terms in the numerator and denominator of Eq. (4d) must dominate. In the numerator of Eq. (4d) this implies $X(^{12}CO)$ well above 2×10^{-6} or that $g_{12} < 0.1$ in Eq. (4c); photodissociation remains the dominant mechanism of CO destruction well into the regime where fractionation is important. For $g_{12}I = 1/33$, $n(H_2) = 40$ cm^{-3}, $T_K = 40$ K, $X(^{12}CO) = 4 \times 10^{-6}$. If the disparity between the isotopic shielding terms is a factor of a few, $Ig_{13} \approx 0.07$–0.1, and dominance of the righthand term in the denominator would require $n(H_2) \gg 150$ cm^{-3}. Thus, although there is substantial creation of ^{13}CO via isotope exchange, it does not occur in a portion of parameter space where the isotope insertion actually equilibrates, creating a reliable gas thermometer.

5.3. What do we learn from $^{12}CO/^{13}CO$ ratios?

Figure 4 shows the observed CO abundance ratios plotted against $X(^{12}CO)$ along with the results of some toy models following the expressions in Eqs. (4c) and (4d), along with the additional parametrization $g_{13} = g_{12}^{0.6}$. The parameter having the greatest influence on the observed isotope ratio is the external photodissociation rate, rather than the density or temperature. In detail, these observations are very hard to interpret in terms of either the detailed physical properties of the gas or the intrinsic carbon isotope ratio. The old hope that CO fractionation would serve as a reliable thermometer is not fulfilled.

However, in very general terms it does appear that the isotopic abundance ratios seen in carbon monoxide can be understood in terms of relatively mundane chemical and photoprocesses in quiescent gas of moderate density, even if it is difficult to derive the underlying physical conditions from the ratios themselves. This is analogous to the recognition that CO can form in the observed quantities from the quiescent thermal gas phase electron recombination of the observed amounts of HCO^+, and in very great contrast to considerations of the abundances of HCO^+ and most other molecular species observed in diffuse gas, certainly all the polyatomics and many diatomics like CS, whereby quiescent models fail by very large factors.

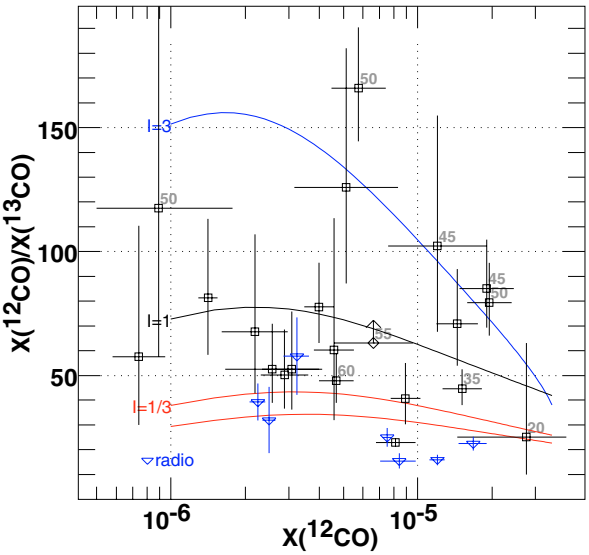

Fig. 4. Variation of $N(^{12}CO)/N(^{13}CO)$ with $X(CO) = N(^{12}CO)/N(H_2)$ compared with the model chemistry (curves) described in Sect. 4.5 of the text. Models are for $I = 3$, $T_K = 45$ K, $n(H_2) = 50$ cm^{-3}; $I = 1$, $T_K = 45$ K, $n(H_2) = 125$ cm^{-3}; $I = 1/3$, $T_K = 22.5$ K, $n(H_2) = 125$ cm^{-3} (upper of two curves) and 250 cm^{-3}. As in Fig. 3 optical data are labelled with the kinetic temperature derived from C_2 as tabulated by Sonnentrucker et al. (2007).

6. $J = 1$–0 rotational excitation and line brightness

6.1. Observed rotational excitation

In optical absorption, carbon monoxide rotational excitation temperatures are derived directly from measurements of column densities in individual rotational levels (Burgh et al. 2007; Sonnentrucker et al. 2007) and $N(H_2)$ is generally known. At mm-wavelengths, the measurements are of optical depths and line brightnesses in rotational transitions (Liszt & Lucas 1998) and the H_2 column density is inferred indirectly, by assuming $N(HCO^+)/N(H_2) = 2 \times 10^{-9}$.

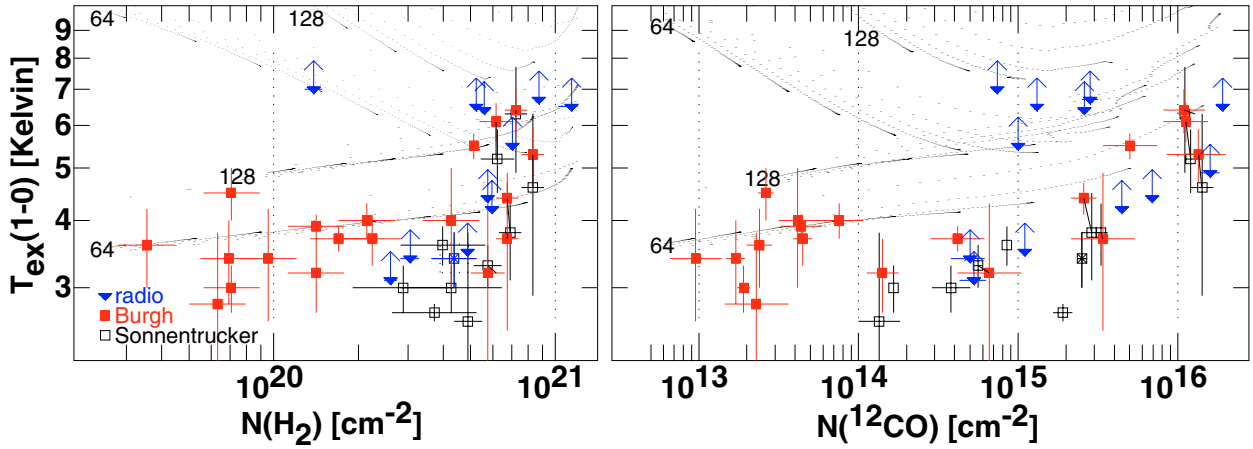

Fig. 5. Variation of ^{12}CO $J = 1-0$ rotational excitation temperature plotted against $N(H_2)$ (*left*) and $N(^{12}CO)$. Radio data are shown as lower limits because they involve the assumption of a beam efficiency. Data from the work of Burgh et al. (2007) and Sonnentrucker et al. (2007) are shown separately; sightlines with measurements in both references are shown chained, note that the former typically derives slightly stronger excitation in these cases. Data labelled "radio" are those of Liszt & Lucas (1998). Superposed on the data are calculated results for uniform-density spherical models having total densites $n(H) = 64$ and 128 cm^{-3} like those used to determine $N(CO)$ in Fig. 1, where only a handful of the sightlines represented here require $n(H) < 64$ cm^{-3}. The lower curves at each density employ an older but likely more nearly correct set of rotational excitation rates for H-atom + CO collisions (see Sect. 6 of the text). A minimum excitation temperature of 4.0 K is required to produce a λ2.6 mm emission line having a brightness temperature $T_B = 1$ K.

Shown in Fig. 5 are $J = 1-0$ rotational excitation temperatures $T_{ex}(1-0)$ from these references. They are very nearly unanimous in showing (at left) that lines of sight with $N(H_2) \lesssim 5 \times 10^{20}$ cm^{-2} have $T_{ex}(1-0) \lesssim 4$ K; 4.0 K is the smallest excitation temperature capable of producing a 1.0 K brightness temperature above the cosmic microwave background (CMB) in the λ2.6 mm $J = 1-0$ line. The same data are plotted against $N(^{12}CO)$ at right in Fig. 5, where some disparity occurs between the radio and optical absorption data; a few lines of sight having $N(^{12}CO) \approx 10^{15}$ cm^{-2} exhibit somewhat brighter $J = 1-0$ lines than would be allowed by a 4 K excitation temperature.

Figure 6 shows the observations recast as integrated λ2.6 mm $J = 1-0$ rotational brightness temperatures $W_{CO} = \int T_B(1-0)dv$. At radio wavelengths, these are directly observed to within a scale factor, the beam efficiency. For optical absorption data, the line brightness can be crafted from the rotational level populations, which fix the integrated optical depth; the central optical depth is then specified by the b-parameter, so that the line brightness can be integrated over the profile. For optically thin lines the integrated brightness is independent of the b-value, but many of the lines of sight with $N(^{12}CO) > 10^{15}$ cm^{-2} observed in uv absorption are predicted to be somewhat opaque at λ2.6 mm, in keeping with direct measurements shown by Liszt & Lucas (1998). For $T_{ex}(1-0) = 2.73$ K or 4.0 K, the integrated optical depth of the $J = 1-0$ transition is 1 km s^{-1} when $N(^{12}CO) = 1.0$ or 1.6×10^{15} cm^{-2}. Finally, note that Burgh et al. (2007) published only $N(^{12}CO)$ and $T_{ex}(1-0)$; to specify the rotational level populations fully we assumed that the excitation temperatures of higher-lying levels were the same as that of the $J = 1-0$ line. The excitation is weak enough that this is not a major problem, little population exists in levels above $J = 2$.

At left, Fig. 6 shows the integrated brightness temperature and H_2 column density for the optical absorption data. Also shown are the predicted (Sonnentrucker et al. 2007) and observed (Liszt 1997) brightnesses toward ζ Oph; the excitation temperature derived by Sonnentrucker et al. (2007) is noticeably smaller than earlier values (Smith et al. 1978; Wannier et al. 1982) leading to a low predicted W_{CO} and larger implied optical depth in the $J = 1-0$ line. Corresponding data comparing W_{CO} and $N(HCO^+)$ were not provided by Lucas & Liszt (1998), so, to test the consistency of the optical and mm-wave results, as elsewhere in this work, we used a set of unpublished, very sensitive, low galactic latitude CO emission and HCO^+ absorption profiles and simply compared the integrated CO brightness and HCO^+ optical depths, scaling the latter appropriately to form $N(HCO^+)$ and $N(H_2)$ as done by Lucas & Liszt (1998) and Lucas & Liszt (1996). This is the one exception noted in Sect. 2 to the use of previously-published data. In any case, it can be seen from Fig. 6 at left that the radio and optical data show the same behaviour.

This comparison of W_{CO} and $N(H_2)$ is tantamount to specifying the CO-H_2 conversion factor; indeed, this regime is really the only one in which the conversion factor may be derived from direct measurement of the two constituents. Clearly the ratio of $N(H_2)/W_{CO}$ is typically very large for weak-lined diffuse CO-bearing gas, compared with the usually assumed local values $N(H_2)/W_{CO} = 2-3 \times 10^{20} H_2$/K-km s^{-1}. However, for sightlines of sight with $W_{CO} > 1$ K km s^{-1}, the ratio is nearly canonical or perhaps a bit low. This insight, that the CO-H_2 conversion factor attains nearly its canonical values at rather small $N(CO)$ was at the heart of the original discussion of Liszt (1982).

The plot of W_{CO} vs. $N(^{12}CO)$ at right in Fig. 6 shows a well-defined proportionality, as noted earlier (Fig. 12 of Liszt & Lucas 1998) and there is good agreement between the optical and radio data when CO emission was actually detected at λ 2.6 mm, at $N(^{12}CO) > 6 \times 10^{14}$ cm^{-2}. Apparently, W_{CO} is a fairly robust and accurate estimator of the CO column density itself and scatter in the CO-H_2 conversion factor arises from the vagaries of the chemistry. Note that Fig. 6 at right reverts to use of the previously published mm-wave data.

For $N(^{12}CO) \approx 3-5 \times 10^{15}$ cm^{-2} the brightness saturates at $W_{CO} \approx 3-6$ K km s^{-1} as the lines become very optically thick. This highlights the fact that the transition to complete C→CO conversion must occur over a relatively small range of $N(H_2)$; if diffuse cloud lines of sight commonly show $J = 1-0$ lines of several K, not grossly different from typical dark gas even when only a few percent of the free carbon is in carbon monoxide, and if the CO-H_2 conversion factor is about the same for dark and brighter-lined diffuse gas, it follows that there must

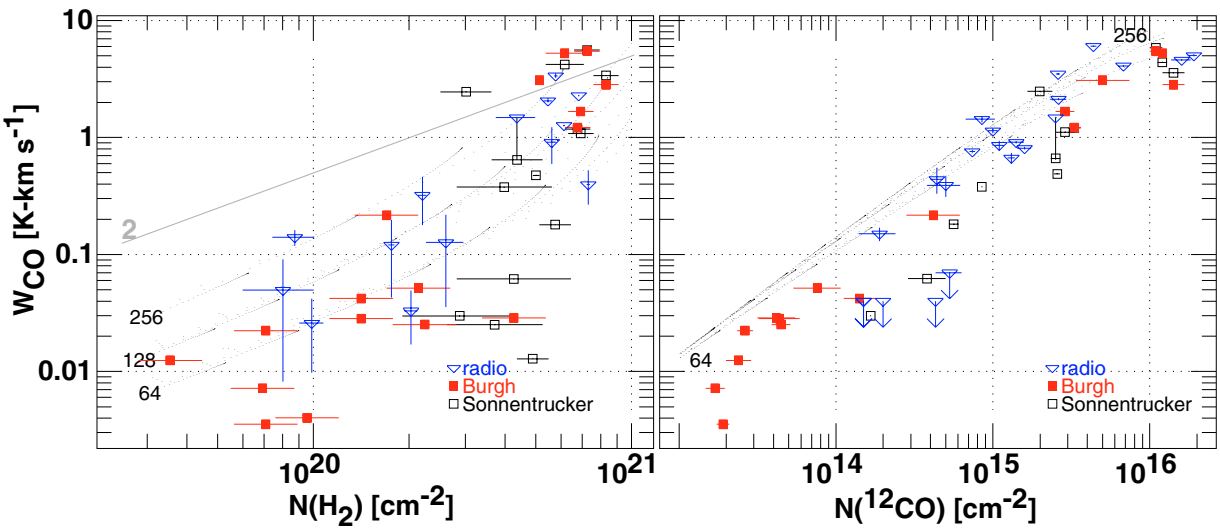

Fig. 6. Integrated ^{12}CO $J = 1-0$ λ2.6 mm brightness temperatures predicted from *uv* absorption and/or observed at λ2.6 mm, plotted against $N(H_2)$ (*left*) and $N(^{12}CO)$ (*right*). The shaded line at left represents a CO-H_2 conversion factor $N(H_2) = 2 \times 10^{20}$ cm^{-2}/K-km s^{-1}. Direct radio observations toward ζ Oph are also shown chained to the equivalent optical datapoint. Data from the work of Burgh et al. (2007) and Sonnentrucker et al. (2007) are shown separately and the radio observations are those of (Liszt & Lucas 1998) at right; see Sect. 6.1 for an explanation of the radio data plotted at left.

be a very rapid increase of X(CO) over a very small interval in $N(H_2)$ and W_{CO}, over and above that seen in Fig. 1.

6.2. Interpretation of the rotational excitation

Until recently, it seemed appropriate to neglect the contribution of excitation by H-atoms, for which the cross-sections were calculated to be relatively small (Green & Thaddeus 1976), to assume a largely molecular host gas, and to use the CO $J = 1-0$ rotational excitation temperature as a probe of the ambient thermal pressure; it could be shown from calculations that there was a nearly linear increase of $T_{ex}(1-0)$ with $n(H_2)T_K$ (Smith et al. 1978; Liszt 1979; Liszt & Lucas 1998) as long as $T_{ex} \ll T_K$. This variation of $T_{ex}(1-0)$ with the ambient thermal pressure of H_2 presumably occurs as a result of the small permanent dipole moment of CO since the excitation of other species with higher dipole moments is typically sensitive mostly to density. However, a recent calculation of the rotational excitation rates of CO by H-atoms yielded the result that the per-particle excitation by hydrogen atoms was much stronger than by H_2 (Balakrishnan et al. 2002). In this case even a small admixture of H-atoms can have a marked effect on the excitation of CO (Liszt 2006) and it is not allowable to derive the ambient thermal partial pressure of H_2 directly from $T_{ex}(1-0)$ by assuming a purely molecular host gas.

As this manuscript was being revised, it was learned (Stancil, private communication; Shepler et al. 2007) that the calculation of Balakrishnan et al. (2002) had been reconsidered and that the older, smaller H-atom excitation rates were in fact more nearly appropriate. Results for both sets of rates are shown here. The choice of excitation rates has several interesting consequences for the interpretation, as noted below.

Model results for the CO excitation are superposed In Figs. 5 and 6. These were calculated by running models (like those used to calculate N(CO) in Fig. 1) at fixed n(H) (as indicated in the figures) and N(H) toward the center, plotting results from sightlines having impact parameters ranging from the outer edge to center. For each model of given n(H) and N(H), the rotational level populations were integrated for each sightline and the result plotted as a point in the figure. Results for n(H) below 64 cm^{-3} are not shown because only a handful of the sightlines represented in Fig. 5 are compatible with $n(H) < 64$ cm^{-3} in Fig. 1 (where they are shown outlined and in green to make just this point).

Shown in Fig. 5 are results for models having $n(H) = 64$ and 128 H-nuclei cm^{-3} using the H-atom excitation rates of Green & Thaddeus (1976) (as approximated by Warin et al. 1996) and those of Balakrishnan et al. (2002). The models include excitation by atomic H and He, and ortho and para-H_2 and the effects of photon-trapping were calculated in the microturbulent approximation for a b-parameter of 0.8 km s^{-1}. The characteristic shape of the upper three curves in Fig. 5 is determined by an increase in the fraction of atomic H toward the left, and by resonant photon-trapping at higher optical depth toward the right. With strong excitation by atomic hydrogen, calculated values of $T_{ex}(1-0)$ increase with n(H) at small $N(H_2)$ or $N(^{12}CO)$. Models using the older cross-sections for excitation by atomic hydrogen do not exhibit such an increase because the overall excitation is weak when the molecular fraction is small.

Only if the smaller H-atom excitation rates are appropriate will the models used to calculate X(CO) also do an acceptable job of reproducing the observed excitation at like density. The excitation temperatures derived from the *uv* absorption data are a bit lower than before, but mostly there is the problem that the fraction of gas which remains in atomic form in the models (which self-consistently determine the local H_2 density) is large enough to have a profound effect on the excitation. Lines of sight with the smallest $N(H_2)$ and $X(^{12}CO)$ are expected to have formed CO in the least purely molecular gas and therefore to show the highest excitation temperatures, opposite to what is observed, if the rates of Balakrishnan et al. (2002) are employed. Except perhaps for the anomalous-seeming radio data near $N(^{12}CO) = 10^{15}$ cm^{-2} at the right in Fig. 5, the calculated rotational excitation is far too high, mainly due to the admixture of residual atomic hydrogen in the CO-bearing regions.

The situation with respect to the integrated brightness shown in Fig. 6 is clearer, as the models actually account quite well for the variation of W_{CO} with $N(H_2)$ at left and they only slightly

overestimate the run of W_{CO} with $N(^{12}CO)$. Furthermore, the calculated values of W_{CO} are not strongly dependent on which set of cross-sections for excitation by H atoms is used. This implies that it may be possible to calculate the CO-H_2 conversion factor reliably, although it should be stressed that the models form CO rather artificially. Moreover, if the larger H-atom excitation rates of Balakrishnan et al. (2002) are employed, the disparity in the ability of the models to account for both T_{ex} and W_{CO} implies that the calculated optical depths are much lower than those which are actually observed at $\lambda 2.6$ mm or inferred from the *uv* absorption data.

7. Loose ends and unanswered questions

The comparison of CO with H_2 in diffuse clouds can now be based on a dataset which far exceeds that for any other trace molecule. Over the diffuse regime, the run of $N(CO)$ with $N(H_2)$ actually seems more consistent and understandable than that of CH, which suffers from an unexplained decline in its relative abundance at $N(H_2) < 7 \times 10^{19}$ cm^{-2} (see Fig. 1); at higher $N(H_2)$, $N(CH)/N(H_2) \approx 4 \times 10^{-8}$ with relatively small scatter. Further observations of CH and other species are required in the regime of moderate $N(H_2)$ and nascent polyatomic chemistry.

On average, the mean $N(^{12}CO)/N(^{13}CO)$ ratio is near the local interstellar isotope ratio $[^{12}C]/[^{13}C] = 60$, but fractionation effects cause the $N(^{12}CO)/N(^{13}CO)$ to vary between 20 and 170 with lower values at somewhat higher $N(^{12}CO)$. The fraction of free gas-phase ^{13}C in ^{13}CO is large enough in some cases that other species sharing the same volume must be somewhat starved for ^{13}C, artificially biasing the ratio of their ^{12}C- and ^{13}C-bearing variants. However, the effects of sharply-varying fractionation might perhaps be most pernicious for mm-wave emission studies, which typically rely on ratios of brightness temperatures in ^{12}CO and ^{13}CO, coupled with the assumption of a fixed abundance ratio $N(^{12}CO)/N(^{13}CO)$, to infer ^{12}CO optical depths, excitation temperatures and column densities. Unrecognizable systematic variations in $N(^{12}CO)/N(^{13}CO)$ could wreak havoc with interpretation of such datasets.

At the present time it is unclear whether fractionation in CO can be regarded as anything more than a nuisance: the observed $N(^{12}CO)/N(^{13}CO)$ ratios result from several competing influences including direct formation, carbon isotope exchange and selective photodissociation, none of which dominates to the extent that the local temperature or density can be inferred. At least in the *uv* datasets, $^{12}CO/^{13}CO$ ratios have generally been measured along lines of sight having only rather high $X(CO)$ and over a relatively modest range of $N(H_2)$ (see Fig. 2). This may have introduced some bias but interpreting the observations is sufficiently difficult that further discussion of the fractionation may not be rewarding per se. However, study of ^{13}CO may be rewarding for other reasons, especially at higher $N(^{12}CO)$ and $N(H_2)$ as more complete carbon conversion to CO occurs.

The convergence of the CO-H_2 conversion factor for diffuse and dark gas well within the diffuse regime (at $N(CO) \lesssim 10^{16}$ cm^{-2} in Fig. 6 at left) suggests that the full conversion of carbon to CO must occur over a very narrow range of extinction, $N(H_2)$, etc. just beyond the diffuse regime. This may leave very little room in parameter space for a "translucent" regime in which neutral carbon is the dominant carbon-bearing species. Given that the CO abundance in dark gas is typically found to be $X(CO) = 8{-}10 \times 10^{-5}$, some 3–4 times smaller than $2[C]/[H] \approx 3.2 \times 10^{-4}$ in diffuse gas, we are left to ask just where the transition from diffuse to dark gas actually occurs in terms of $N(H_2)$ and what is the carbon budget in the transition regime.

In the diffuse regime, the CO-H_2 conversion factor is actually measured and found to attain values $N(H_2)/W_{CO} = 2{-}3 \times 10^{20} H_2/\text{K-km s}^{-1}$ along rather thin lines of sight where the fraction of free gas-phase carbon in CO is only a few percent. These lines of sight also have W_{CO} of a few K-km s^{-1}, as is typical of darker material. Again we are left to wonder how much room in parameter space is actually left for a translucent regime.

The observed CO-H_2 conversion factors and CO $J = 1{-}0$ rotational line brightnesses are actually well-explained by the uniform density models whose results are presented in Figs. 1, 5 and 6. The most notable possible failure in the interpretation here is the mismatch between the too-large excitation temperatures and too-small optical depths predicted by the models for the $J = 1{-}0$ rotational transition (see Fig. 5 at left) when the recent calculation of the H-atom + CO excitation rates by Balakrishnan et al. (2002) is employed (see Sect. 6.2). The models are uniform and rather diffuse and so leave a substantial fraction of H-nuclei in atomic form in some cases. Excitation by such H atoms was ignorable using older excitation rates (Green & Thaddeus 1976) but the rates of Balakrishnan et al. (2002) are so large that even a slight amount of residual atomic hydrogen would have a profound effect. Although the disagreement between observed and measured excitation temperatures seems to point to the need to sequester CO in regions of nearly pure H_2, the agreement is actually worst for the most diffuse gas with the smallest $N(CO)$ and $X(CO)$. Should such gas really be expected to be the most purely molecular? Perhaps the neatest way around this problem lies with the apparent recent realization that the older, smaller excitation rates by H atoms are actually more nearly correct. In this case the models do a good job of reproducing the rotational excitation of CO at the same densities at which CO forms, even if the ambient hydrogen is not exclusively molecular.

There is little difference in ^{12}CO $J = 1{-}0$ line brightness between dark clouds with $X(^{12}CO) = 10^{-4}$, $N(^{12}CO) = 3{-}10 \times 10^{17}$ cm^{-2} and that from diffuse clouds with $X(^{12}CO) = 2 \times 10^{-5}$, $N(^{12}CO) = 3{-}10 \times 10^{15}$ cm^{-2}. Although dark and diffuse gas may better be distinguished on the basis of observations of ^{13}CO (acknowledging possible effects of fractionation) or $C^{18}O$, such data are not always available. Given the prevalence of diffuse gas at larger distances from the center of the Galaxy and larger distances from the galactic plane, it seems worthwhile to ask whether possible confusion between diffuse and dark gas has caused misjudgement of the quantity and character of molecular gas in our own or other galaxies.

Acknowledgements. The National Radio Astronomy Observatory is operated by Associated Universites, Inc. under a cooperative agreement with the US National Science Foundation. I am grateful to Phillip Stancil for informing me of the very recent calculations of CO excitation by H atoms due to Shepler et al. (2007) and to Malcolm Walmsley for a host of worthwhile comments. The finishing touches were put on this paper while the author was enjoying the hospitality of IRAM and the Hotel Hesperia in Granada.

References

Abrahamsson, E., Krems, R. V., & Dalgarno, A. 2007, ApJ, 654, 1171
Balakrishnan, N., Yan, M., & Dalgarno, A. 2002, ApJ, 568, 443 (BYD)
Burgh, E. B., France, K., & McCandliss, S. R. 2007, ApJ, 658, 446
Chu, Y.-H., & Watson, W. D. 1983, ApJ, 267, 151
Crenny, T., & Federman, S. R. 2004, ApJ, 605, 278
Dessauges-Zavadsky, M., Combes, F., & Pfenniger, D. 2007, [arXiv:0708.1120]
Federman, S. R., Lambert, D. L., Sheffer, Y., et al. 2003, ApJ, 591, 986

Gredel, R., van Dishoeck, E. F., & Black, J. H. 1993, A&A, 269, 477
Green, S., & Thaddeus, P. 1976, ApJ, 205, 766
Lambert, D. L., Sheffer, Y., Gilliland, R. L., & Federman, S. R. 1994, ApJ, 420, 756
Langer, W. D., Graedel, T. E., Frerking, M. A., & Armentrout, P. B. 1984, ApJ, 277, 581
Le Teuff, Y. H., Millar, T. J., & Markwick, A. J. 2000, aas, 146, 157
Lee, H. H., Herbst, E., Pineau Des Forets, G., Roueff, E., & Le Bourlot, J. 1996, A&A, 311, 690
Liszt, H. 2003, A&A, 398, 621
Liszt, H., & Lucas, R. 2002, A&A, 999, 888
Liszt, H. S. 1979, ApJ, 233, L147
Liszt, H. S. 1982, ApJ, 262, 198
Liszt, H. S. 1997, A&A, 322, 962
Liszt, H. S. 2006, A&A, 458, 507
Liszt, H. S. 2007, A&A, 461, 205
Liszt, H. S., & Lucas, R. 1994, ApJ, 431, L131
Liszt, H. S., & Lucas, R. 1996, A&A, 314, 917
Liszt, H. S., & Lucas, R. 1998, A&A, 339, 561
Liszt, H. S., & Lucas, R. 2000, A&A, 355, 333
Lucas, R., & Liszt, H. 1998, A&A, 337, 246
Lucas, R., & Liszt, H. S. 1996, A&A, 307, 237
Lucas, R., & Liszt, H. S. 2000, A&A, 355, 327
McCall, B. J., Hinkle, K. H., Geballe, T. R., et al. 2002, ApJ, 567, 391
Sheffer, Y., Rogers, M., Federman, S. R., Lambert, D. L., & Gredel, R. 2007, ApJ, 667, 1002
Shepler, B. C., Yang, B. H., Dhilip Kumar, T. J., et al. 2007, A&A, 475, L15
Smith, A. M., Stecher, T. P., & Krishna Swamy, K. S. 1978, ApJ, 220, 138
Smith, D., & Adams, N. G. 1980, ApJ, 242, 424
Snow, T. P., & McCall, B. J. 2006, ARA&A, 44, 367
Sofia, U. J., Lauroesch, J. T., Meyer, D. M., & Cartledge, S. I. B. 2004, ApJ, 605, 272
Sonnentrucker, P., Welty, D. E., Thorburn, J. A., & York, D. G. 2007, ApJS, 168, 58
Van Dishoeck, E. F., & Black, J. H. 1988, ApJ, 334, 771
Wannier, P. G., Penzias, A. A., & Jenkins, E. B. 1982, ApJ, 254, 100
Warin, S., Benayoun, J. J., & Viala, Y. P. 1996, A&A, 308, 535
Watson, W. D., Anicich, V. G., & Huntress, W. T. J. 1976, ApJ, 205, L165
Welty, D. E., Hobbs, L. M., & Morton, D. C. 2003, ApJS, 147, 61
Woodall, J., Agúndez, M., Markwick-Kemper, A. J., & Millar, T. J. 2007, A&A, 466, 1197
Zsargó, J., & Federman, S. R. 2003, ApJ, 589, 319